ResearchGate

See discussions, stats, and author profiles for this publication at: https://www.researchgate.net/publication/231659670

Hydrogen Bonding in Supercritical Water. 2. Computer Simulations

ARTICLE *in* THE JOURNAL OF PHYSICAL CHEMISTRY A · DECEMBER 1997

Impact Factor: 2.69 · DOI: 10.1021/jp971218j

CITATIONS
125

READS
32

2 AUTHORS:

Andrey G. Kalinichev
École des Mines de Nantes
117 PUBLICATIONS **2,917** CITATIONS
SEE PROFILE

Jay Bass
University of Illinois, Urbana-Champaign
212 PUBLICATIONS **4,911** CITATIONS
SEE PROFILE

Available from: Jay Bass
Retrieved on: 24 January 2016

Hydrogen Bonding in Supercritical Water. 2. Computer Simulations

A. G. Kalinichev*,† and J. D. Bass

Department of Geology, University of Illinois at Urbana−Champaign, 1301 W. Green Street, 245 NHB, Urbana, Illinois 61801

Received: April 9, 1997; In Final Form: October 2, 1997[⊗]

Monte Carlo computer simulations were performed under thermodynamic conditions corresponding to available X-ray and neutron diffraction measurements of the supercritical water structure. A detailed analysis of hydrogen bonding in supercritical water is presented, based on the recently proposed hybrid distance−energy criterion of H-bonding. Good agreement is found with all available experimental and computer simulated results. With increasing temperature, the average number of H-bonds per a water molecule, $\langle n_{HB} \rangle$, decreases with the same slope for both high-density (∼1.0 g/cm^3) as well as low-density (∼0.2 g/cm^3) supercritical water, asymptotically approaching zero at higher temperatures and lower densities. Over the whole supercritical region, except for the highest density states, $\langle n_{HB} \rangle$ is always below the percolation threshold (∼1.6), indicating that the continuous network of hydrogen bonds is broken. Nevertheless, even at the highest temperature and the lowest density simulated, some degree of hydrogen bonding is still present in the form of dimers and trimers. For supercritical conditions of 673 K and 0.66 g/cm^3, average hydrogen bonds are almost 10% weaker, 5% longer, and about 8° more bent, compared to those in normal liquid water. However, over 40% of them are still preserved in the supercritical state, in good aggreement with estimates from all available experimental data.

I. Introduction

Supercritical water (i.e., water at temperatures and pressures above the critical point, $T_c = 647$ K = 374 °C; $P_c = 22.1$ MPa) has recently become a subject of growing scientific interest due to its crucial role in a variety of natural processes (e.g., those taking place in so-called hydrothermal systems[1,2]), as well as because of emerging technological applications.[3,4] Due to the large compressibility of supercritical fluids, small changes in pressure can produce substantial changes in density, which, in turn, affect diffusivity, viscosity, dielectric, and solvation properties, thus dramatically influencing the kinetics and mechanisms of chemical reactions in water.

It is also well-known that many anomalous properties of water are the consequence of specific hydrogen-bonding interactions of its molecules. The question of the ranges of temperature and density where these specific interactions can significantly influence the observable properties of water substance is very important for the construction of realistic structural models for this fluid.[5] Experimental evidence suggests that some degree of H-bonding persists well into the supercritical region.[6,7] However, the direct experimental investigation of the supercritical water structure is a very challenging task, and any new structural information obtained at high temperatures and pressures is extremely valuable. The latest series of experiments by Soper et al.[8−10] represent a very important step forward in introducing into the field the powerful technique of neutron diffraction with isotope substitution (NDIS), since this method allows one to experimentally probe all three atom−atom structural correlations in supercritical water (OO, OH, and HH) simultaneously. Recent proton NMR chemical shift measurements by Hoffmann and Conradi[11] represent yet another independent source of experimental information on the degree of hydrogen bonding in water under supercritical conditions.

On the other hand, there are numerous Monte Carlo (MC) and molecular dynamics (MD) computer simulation studies of supercritical water performed over the last decade[12−27] using several effective intermolecular potential functions. The advantage of computer "experiments" in this context is in their ability to generate and analyze in detail spatial and energetic arrangements of every individual molecule or multimolecular configurations in the system, thus providing extremely useful microthermodynamic and microstructural information on the molecular level, not available from any real physical measurement. In addition to that, computer simulations provide usual time- or ansemble-averaged properties of the molecular system, which can be directly compared with experimental data.

Several sources of experimental data were analysed recently,[6] and it was demonstrated that very good consistence exists between estimates of the degree of hydrogen bonding in supercritical water inferred from IR absorption measurements[28−30] as well as from direct structural studies by energy-dispersive X-ray diffraction technique.[31−33] This latter set of structural data for some reason was not included in the recent comparisons of experimental and computer simulated supercritical water structure.[10,20,22,24,27] In the present paper we report the results of MC computer simulations performed under thermodynamic conditions corresponding to those of X-ray[31−33] as well as neutron[8−10] diffraction experiments. We also compare these results with some other simulations under similar thermodynamic conditions.[23,34]

Technical details of the Monte Carlo simulations are presented in section II, along with some brief discussion of thermodynamic results. The structure of supercritical water in terms of atom−atom radial distribution functions is discussed next in section III. In section IV we present a detailed analysis of hydrogen-bonding statistics in supercritical water based on the proposed intermolecular distance−energy distribution functions and compare the results with all available experimental data. The conclusions of the present study are briefly summarized in the last section V.

† Present address: Institute of Experimental Mineralogy, Russian Academy of Sciences, 142432 Chernogolovka Moscow Region, Russia (E-mail: andreyk@iem.ac.ru).

⊗ Abstract published in *Advance ACS Abstracts,* November 15, 1997.

S1089-5639(97)01218-8 CCC: $14.00 © 1997 American Chemical Society

TABLE 1: Thermodynamic Properties of Sub- and Supercritical TIP4P Water

T/K:	573	573	573	573	573	673	673	673	673
P/MPa:	9.5	30	50	80	100	50	80	100	130
ρ/g·cm^{-3}	0.0576(4)[a]	0.627(2)	0.669(2)	0.722(2)	0.754(2)	0.393(3)	0.542(4)	0.601(2)	0.655(2)
	0.7145[b]	0.7508	0.7565	0.8066	0.8233	0.5778	0.6595	0.6929	0.7307
H_{conf}/kJ·mol^{-1}	−3.95(1)	−23.93(9)	−24.33(6)	−24.66(6)	−24.89(5)	−14.90(10)	−17.93(10)	−18.76(6)	−19.30(7)
	−26.46	−26.73	−26.81	−26.79	−26.72	−19.72	−20.90	−21.22	−21.43
C_P/J·mol^{-1}·K^{-1}	122(5)	117(6)	96(4)	93(4)	83(3)	123(6)	111(5)	88(3)	85(3)
	103	91.5	86.1	81.4	79.3	122.4	94.9	88.3	82.5
$\kappa \times 10^3$/MPa^{-1}	170(10)	6.6(6)	3.2(2)	2.4(2)	1.6(1)	16.3(10)	7.3(6)	3.6(2)	2.5(2)
	3.10	1.95	1.47	1.10	0.95	7.17	2.91	2.1	1.5
$\alpha \times 10^5$/K^{-1}	775(50)	510(45)	295(20)	256(20)	195(10)	625(50)	452(30)	271(15)	224(15)
	320.2	229.4	188.3	153.7	138.7	491.2	265.1	213.7	171.2

[a] Statistical uncertainties in the last significant figures are given in parentheses. [b] In the second row the values calculated from the equation of state[38] are given for comparison as "experimental".

II. Monte Carlo Simulations

Isothermal−isobaric MC simulations were performed for a system of $N = 216$ water molecules in a cubic cell with periodic boundary conditions. A conventional *NPT* ensemble algorithm[35] used in the simulation is described in detail elsewhere.[14] Water molecules were interacting via the effective site−site pair potential TIP4P,[36] which uses the experimental rigid geometry of the monomer (OH bond length = 0.9572 Å and ∠HOH = 104.52°) and has four interaction sites: three on the nuclei and one on a point M located on the bisector of the HOH angle at a distance of 0.15 Å from the oxygen toward the hydrogens. Two charges of 0.52*e* are located on the hydrogens, compensated by the charge −1.04*e* on M. The total interaction energy for a pair of molecules consists of the Coulomb interactions between the charged sites and a Lennard-Jones interaction between the oxygen atoms, with the parameters $\sigma = 3.154$ Å and $\epsilon/k = 78.1$ K in conventional LJ units.[36]

Over 30 thermodynamic states were simulated for liquid and supercritical water at temperatures between 273 and 1273 K over a pressure range from 10 to 10 000 MPa, thus sampling a very wide density range between 0.02 and 1.67 g/cm^3. For each thermodynamic state the properties were averaged over 10^7 equilibrium MC configurations with another 5×10^6 configurations generated and rejected on the preequilibration stage. The convergence of all the properties was monitored during the simulations, and the statistical uncertainties were calculated by averaging over 50 smaller parts of the total chain of configurations.

A detailed analysis of the thermodynamic results of present simulations is given elsewhere.[25,37] Simulated values of density, configurational enthalpy (H_{conf}), isobaric heat capacity (C_P), isothermal compressibility (κ), and thermal expansivity (α) for two isobars of 50 and 100 MPa (where experimental X-ray structural data[31−33] are available) are shown in Figure 1. The values calculated along the two isobars using a standard equation of state for water[38] are also given in Figure 1 as solid lines for comparison. The results demonstrate a remarkable ability of the TIP4P intermolecular potential to accurately reproduce the thermodynamic properties of water over very wide ranges of temperautres and densities. However, as had been noted earlier,[14,25] the shape of the simulated thermodynamic surface in the near-critical region indicates that the critical point for the TIP4P water model is located approximately 50° lower than observed experimentally. The same conclusion can also be drawn by extrapolating the simulation results for TIP4P water along the vapor−liquid coexistence curve.[39]

The simulated thermodynamic properties at 573 and 673 K under the conditions closely corresponding to those of the neutron diffraction experiments[10] are given in Table 1. The simulated results seem to be shifted down in density relative to the experimental[38] values. (The point at 573 K and 9.5 MPa is obviously shifted from liquid to the vapor branch of the isotherm.) This shift is the direct consequence of the above-mentioned shifted location of the critical point for the TIP4P water model and does not create much problems if we use density rather than pressure as an independent variable for comparison.

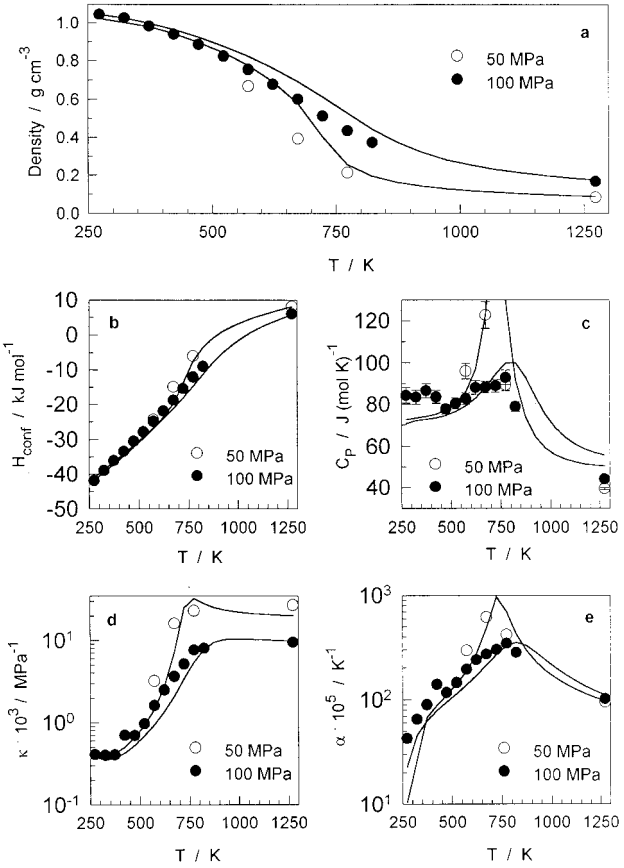

Figure 1. Temperature dependence of density, configurational enthalpy, isobaric heat capacity, isothermal compressibility, and thermal expansivity for TIP4P water along two isobars. Open and filled dots are for 50 and 100 MPa, respectively. Lines are calculated from the equation of state for water.[38]

This qualitatively and quantitatively correct behavior of the simulated thermodynamic properties for the TIP4P water over very wide ranges of temperatures and densities allows us to analyze with reasonable confidence the detailed temperature and density dependence of local spatial and energetic arrangements of water molecules leading to hydrogen bonding.

III. Structure of Supercritical Water

Figure 2 compares the simulated $g_{OO}(r)$ radial distribution functions with the molecular pair correlation functions obtained

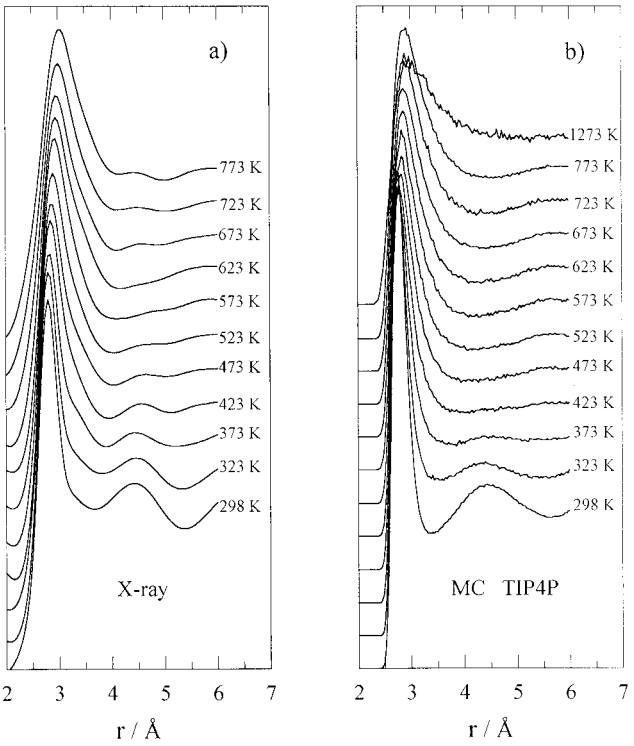

Figure 2. Oxygen−oxygen pair correlation functions of liquid and supercritical water at a constant pressure of 100 MPa. (a) From X-ray diffraction experiments.[33] (b) From Monte Carlo computer simulations using the TIP4P potential.

from the X-ray diffraction measurements[31−33] along the 100 MPa isobar. The general agreement is reasonably good, if we take into account that most of the simulated high-temperature functions correpond to densities lower than experimental, due to the shifted location of the critical point for the TIP4P water model discussed in the previous section. The excessive steepness of the simulated functions in the region around 2.5 Å is a common problem with many effective pair potentials of water[14,17,36,40,41] resulting from the excessive stiffness of the Lennard-Jones-like repulsive interactions.

A more detailed comparison of simulated structural functions for liquid and supercritical water with available neutron and X-ray diffraction data is shown in Figures 3−5. For normal liquid water (Figure 3) the TIP4P potential gives higher and narrower $g_{OO}(r)$ and $g_{OH}(r)$ first peaks, compared to experimental data, which again can be largely attributed to the excessive stiffness of the Lennard-Jones repulsion term. It is also worth noting that in the region below 3 Å the inaccuracy of peak heights derived from neutron diffraction experiments can be as large as 14%, despite the fact that the position of peaks is determined much more accurately.[10] On the other hand, the simulated O−O structure beyond the first-neighbor shell ($r_{OO} > 3.7$Å) coincides with X-ray and neutron diffraction data within experimental error. Note that the two experimental sources give quite different depthts of the first $g_{OO}(r)$ minimum, compensated by some difference in the width of the first peak.

The distinct first peak of $g_{OH}(r)$ at $\sim$ 1.8 Å and the following deep minimum at $\sim$ 2.4 Å are the basis of a simple geometric definition of a hydrogen bond, whereby the bond is taken to exist between a pair of water molecules whose respective O and H atoms are separated by less than 2.4 Å. Via integration under $g_{OH}(r)$ up to the chosen threshold distance this criterion provides often used quantitative estimates of the average number of H-bonds in which an individual molecule participates under various thermodynamic conditions.[13,42] While the TIP4P potential overestimates the height of this first $g_{OH}(r)$ peak and the

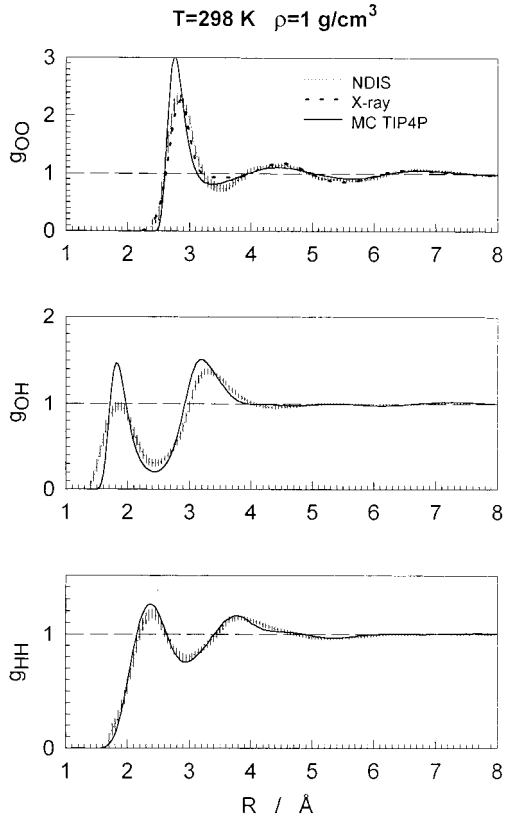

Figure 3. Atom−atom radial distribution functions for liquid water from X-ray diffraction[33] (thick dotted line), neutron diffraction[8,10] (thin dotted lines with error bars), and MC simulations with the TIP4P potential (solid lines).]

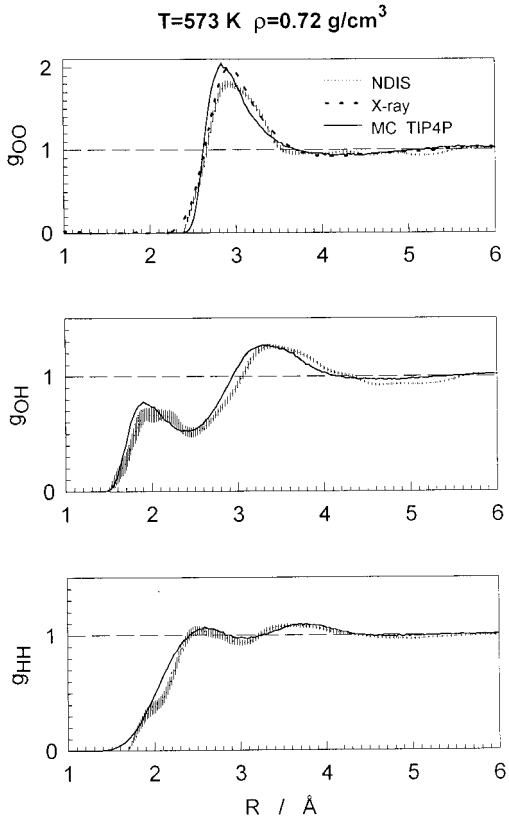

Figure 4. Atom−atom radial distribution functions for subcritical (573 K) water from X-ray diffraction[33] at 0.82 g/cm^3 (thick dotted line), neutron diffraction[10] at 0.72 g/cm^3 (thin dotted lines with error bars), and MC simulations with the TIP4P potential at 0.72 g/cm^3 (solid lines).

depth of the following minimum relative to the neutron data,[8,10] the positions of the $g_{OH}(r)$ extrema are reproduced quite

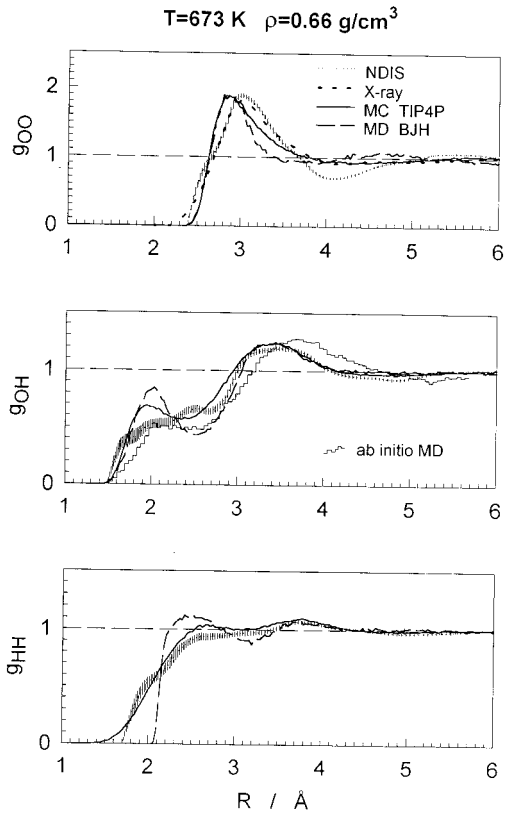

Figure 5. Atom−atom radial distribution functions for supercritical water from present MC simulations with the TIP4P potential at 673 K and 0.66 g/cm^3 (solid lines), X-ray diffraction[33] at 673 K and 0.69 g/cm^3 (thick dotted line), neutron diffraction[10] at 673 K and 0.66 g/cm^3 (thin dotted lines with error bars), MD simulations[23] with the BJH potential[44] at 630 K and 0.69 g/cm^3 (dashed lines), and ab initio MD simulations[34] at 730 K and 0.66 g/cm^3 (thin broken line).

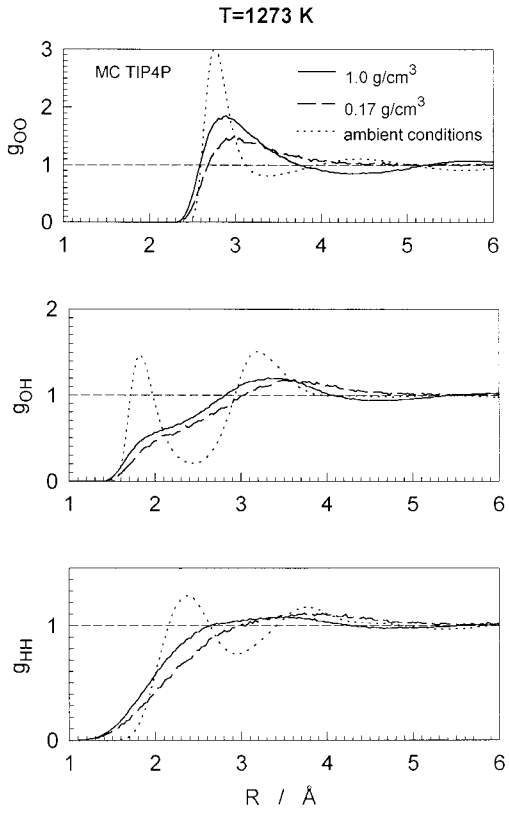

Figure 6. Atom−atom radial distribution functions for high-temperature (1273 K) supercritical water at 1.0 g/cm^3 (full lines) and 0.17 g/cm^3 (dashed lines) from MC simulations with the TIP4P potential.

accurately, and the above-mentioned geometric estimate gives the same average number of H-bonds per water molecule in both cases $\langle n_{HB}\rangle_G = 3.2$. The experimental $g_{HH}(r)$ function (which is the most accurately extracted function from the neutron data) is reproduced by the present TIP4P simulations within experimental error in the entire range of distances.

For the subcritical conditions of Figure 4 the agreement of the simulated $g_{OO}(r)$, $g_{OH}(r)$, and $g_{HH}(r)$ functions with the X-ray[31−33] and neutron[10] data is again very satisfactory. In fact, it is almost within experimental error. The geometric estimates of the hydrogen bonding give $\langle n_{HB}\rangle_G = 2.4$ for both simulated and neutron $g_{OH}(r)$.

The disagreement of simulated and experimental radial distribution functions is somewhat larger at the supercritical temperature of 673 K (Figure 5). Recent results of two other computer simulations[23,34] under very similar thermodynamic conditions are also shown in Figure 5 for comparison. The structural functions simulated by Chialvo and Cummings[20,27] for the SPC/E water model[43] are not shown in Figures 4 and 5 because they virtually coincide with present results for the TIP4P model. Simulations of Mountain[24] for the ST2 and RPOL intermolecular potentials are also very close to the results for other water models.

The most striking feature of the neutron diffraction data in Figure 5 is the disappearance of the first maximum of $g_{OH}(r)$ at ∼2 Å. However, a significant shoulder still remained at its place. This feature is best reproduced by the ab initio MD simulations of Fois et al.[34] where no assumptions on the potential is *a* priori made. Present TIP4P MC simulations also come close to the neutron data, while MD simulations with the flexible BJH water model[44] show much more structure in $g_{OH}(r)$, compared to experimental data. The geometric estimates of $\langle n_{HB}\rangle_G$ again give very close values of 2.1 for both experimental and presently simulated (TIP4P) $g_{OH}(r)$ distribution functions, while they are equal to 2.3 and 1.7 for the BHJ and ab initio MD simulations, respectively.

The presence of an inflection point on the experimental $g_{HH}(r)$ functions at ∼2 Å (see Figures 4, 5) is not reproduced in the simulations. However, the overall agreement between neutron data and present TIP4P simulations for $g_{HH}(r)$ is still quite satisfactory. The BJH potential is unable to correctly reproduce the behavior of this function because it explicitly forbids two hydrogens of different molecules to come closer than 2 Å to each other.[23]

Although the general trends of the correlation functions measured by neutron diffraction (such as the shift to larger distances and the broadening of the first $g_{OH}(r)$ peak with increasing temperature and decreasing density[10,45]) are qualitatively reproduced in the present simulations, these effects are much less pronounced than observed experimentally. Nonetheless, they are clearly seen in Figure 6, where the structural results of two extremely high-temperature (1273 K) MC simulations are shown for liquidlike and gaslike densities of supercritical water. The same functions for liquid water under ambient conditions are also given there for comparison. Figure 6 demonstrates that with increasing temperature and decreasing density the first peak of $g_{OH}(r)$ related to H-bonding disappears due to the shifting and broadening, thus gradually filling the gap in the distribution between 2 and 3 Å, the feature observed from neutron diffraction data even at much lower supercritical temperature (cf. Figures 3−5). With this specific to hydrogen bonding peak becoming much less distinct at high temperatures, the simple geometric criterion of H-bonding based exclusively on the analysis of $g_{OH}(r)$ distribution becomes completely unreliable, and some additional orientational and energy criteria need to be taken into account.[9,10,19,20]

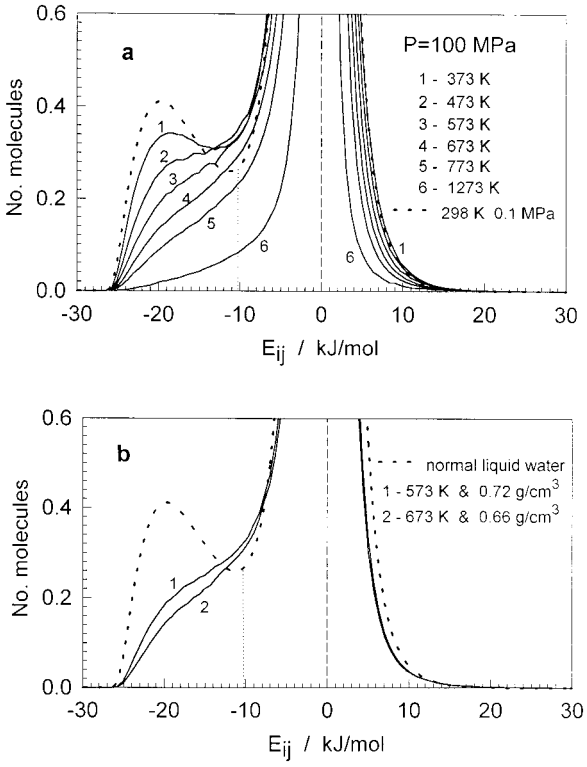

Figure 7. Normalized distributions of pair interaction energies (dimerization energies) in liquid and supercritical water. (a) Temperature dependence at a constant pressure of 100 MPa. (b) Under the thermodynamic conditions where neutron diffraction experiments[10] were performed.

IV. Hydrogen-Bonding Statistics in Supercritical Water

In computer simulations, specific configurations of molecules, which can be considered as hydrogen-bonded, arise as a consequence of the charge distribution on individual water molecules. For a quantitative analysis of the H-bonding, various geometric constraints are often used in addition to the analysis of $g_{OH}(r)$. They are most frequently based on the requirement that one or several internal coordinates of a pair of water molecules (such as oxygen−oxygen distance, angles between some characteristic bond directions) fall within a certain specified range of values.[10,20,24,27,46−48]

There also exists an energetic criterion of a hydrogen bond, which consideres two molecules to be H-bonded if the interaction energy between them is lower than a given negative threshold.[49] This criterion has been successfully applied to the analysis of temperature and density effects on the H-bond distributions in liquid and supercritical water.[19,25,36] In principle, the application of both purely geometric or purely energetic criteria should result in the same physical picture of hydrogen bonding. In practice however, both pictures are not always consistent, especially under supercritical conditions.[19,25]

The selection of the specific threshold energy value in the energetic criterion of hydrogen bonding is based on the analysis of pair energy distributions. These functions represent the probability density of finding a pair of water molecules that have some particular interaction energy under given thermodynamic conditions. They can be routinely calculated in computer simulations. Figure 7 shows such functions for the thermodynamic states where some experimental structural information is available from either X-ray[31−33] or neutron[10] diffraction measurements (cf. Figures 2, 4, 5). Similar distribution for normal liquid water under ambient conditions is also shown in Figure 7 for comparison.

Independent of the thermodynamic conditions, most interactions in the system involve pairs of rather distant molecules, resulting in the main peak of the distribution around 0 kJ/mol. However, under ambient conditions (dashed line in Figure 7a,b), there exists a low-energy peak which is commonly associated with the interactions of hydrogen-bonded neighbors. The minimum of the distribution at about −10 kJ/mol is usually taken as the energetic cutoff threshold (E_{HB}) for hydrogen bonding.[36] The integration under this low-energy peak up to E_{HB} gives us another quantitative estimate of the number of H-bonds per water molecule in the system, which is completely independent of any geometric considerations. However, it can be shown that for normal liquid water this estimate virtually coincides with the simplest geometric estimate based on the analysis of the $g_{OH}(r)$ function.[19]

With increasing temperature and decreasing density the main peak of the distribution becomes narrower with a higher maximum (beyond the scale in Figure 7), because relatively more pairs of molecules are become separated by large intermolecular distances with a near-zero interaction energy. The height of the low-energy peak decreases, but a distinct shoulder is clearly seen at the same range of energies, indicating the noticeable persistence of hydrogen bonding even at the highest temperature and the lowest density.

As it has been previously shown,[49,50] the variation of the energetic threshold value E_{HB}, within reasonable limits, does not qualitatively affect the picture of hydrogen bonding in normal liquid water, which remains remarkably similar for a number of water−water interaction potentials used in simulations.[16,19,26,36,49,50] Thus, adopting the same value of $E_{HB} = -10$ kJ/mol for all thermodynamic states provides a universal and simple criterion for quantifying the picture of H-bonding at any temperature and density. Note that this value of E_{HB} is consistent with spectroscopic and thermodynamic estimates of the hydrogen-bonding energy.[51]

To better visualize the picture of hydrogen bonding, we have recently proposed[19,25] to use intermolecular distance−energy distributions which combine both $g_{OH}(r)$ and E_{ij}, as shown in Figure 8. Each point on the surface of such a distribution represents the relative probability of finding the hydrogen atom of a molecule i at a distance $R_{O\cdots H}$ from the oxygen atom of a molecule j, with a specified interaction energy between the molecules of E_{ij}. It is obvious now from Figure 8a that for normal liquid water either geometric or energetic criteria both quite successfully and consistently distinguish H-bonded molecular pairs from the nonbonded ones, since the former are represented by the distinct low-energy short-distance peak on the distance−energy distribution surface around −20 kJ/mol and 1.8 Å. The feature at the same energy range, but at distances around 3.3 Å represents the most likely positions of the second hydrogen of an H-bonded molecule and corresponds to the second maximum of $g_{OH}(r)$ in Figures 3−6.

Under supercritical conditions (Figure 8b), the picture becomes much more complicated. The nonoverlapping "tails" of the distance−energy distributions extend far beyond the chosen threshold values of HB energy and distance. Some of the molecular pairs considered as bonded in geometric terms can even have positive (repulsive) interaction energy, thus being obviously nonbonded in any reasonable physical sense. On the other hand, molecular pairs considered as H-bonded in energetic terms can have an O···H separation as high as 3.0 Å, which also seems to be unreasonably large.

The simplest geometric criterion of H-bonding based on $g_{OH}(r)$ can, obviously, be made more selective by introducing additional spatial constraints on other interatomic separations and relative orientations of the interacting molecular pairs.[10,20,24,27,46−48] However, this inevitably jeopardizes the simplicity and universality of the criteria by increasing the

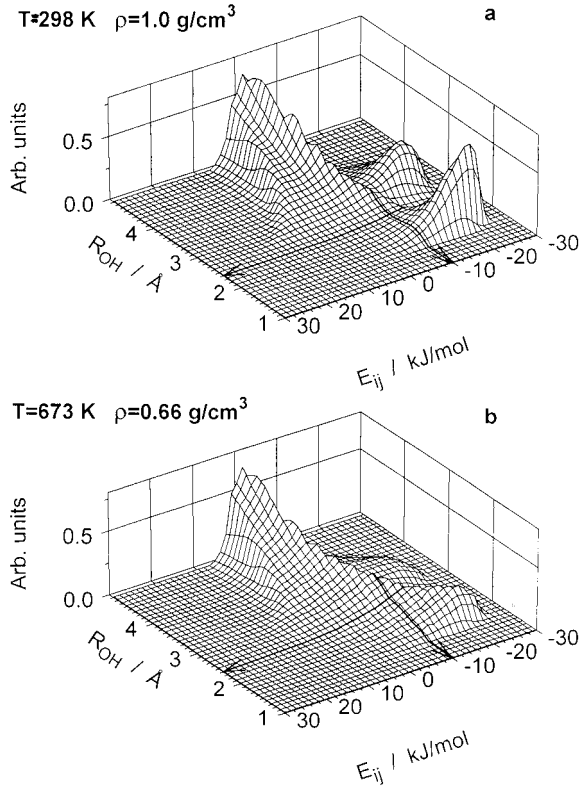

Figure 8. Normalized intermolecular O···H distance−energy distribution functions for liquid (a) and supercritical (b) water. Arrows show the cutoff values of the H-bond definition.

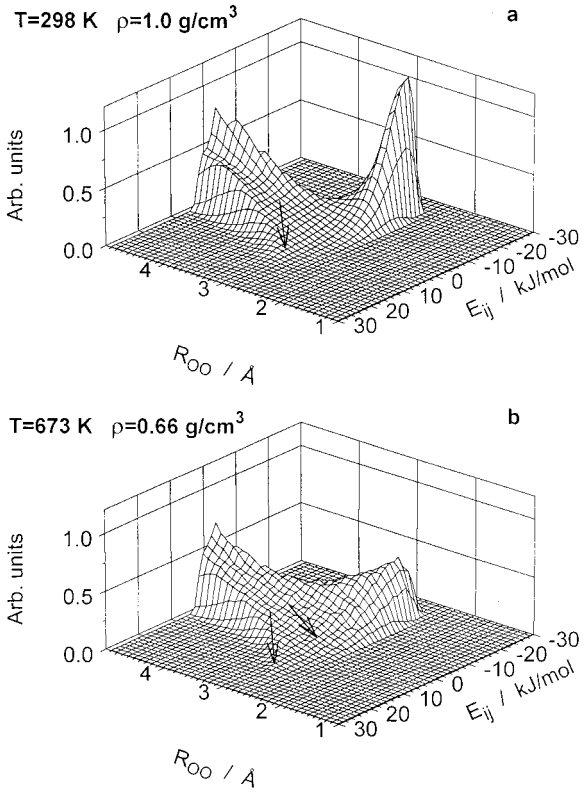

Figure 9. Normalized intermolecular O···O distance−energy distribution functions for liquid and supercritical water. Arrows show the regions where "interstitial" molecules are located.

number of more or less arbitrarily chosen threshold parameters in the analysis. Instead, we suggest simultaneous application of just two intermolecular cutoff criteria—one distance-based ($R_{O\cdots H}$) and one energy-based (E_{ij})—as the best compromise between simplicity and unambiguity of the constraints imposed on any molecular pair to distinguish between H-bonded and non-bonded configurations. In general, any bond is most naturally described in terms of its length and strength, which is directly reflected in the suggested combined criterion. The third very important characteristic of H-bonding under supercritical conditions, namely the lifetime of a bond, cannot be estimated from MC simulations and is, therefore, left beyond the scope of the present paper.[24,26,52]

In Figure 9 distance−energy distributions for the same thermodynamic conditions as in Figure 8 are presented using the intermolecular oxygen−oxygen distance as an independent variable. This distribution is also very informative and allows us to bring additional energetic argumentation to the analysis of experimental radial distribution functions obtained from X-ray diffraction measurements.[6,33] Figure 9 clearly shows that in the first coordination sphere of a water molecule, at the nearest distances as short as 3.0−3.2 Å, there is a significant number of nonbonded, or "interstitial", neighbors having high positive interaction energies. Relative to the number of H-bonded nearest neighbors, and the total number of molecules in the first coordination sphere, the number of these "interstitial" molecules is growing with increasing temperature and decreasing density. Since the interaction energy between a pair of water molecules strongly depends on their mutual orientation (especially at short distances), the observed picture is, in principle, equivalent and complementary to the one obtained from the analysis of spatial angular distribution functions.[8,9,53]

Average energy U_{HB}, distance $R_{O\cdots H}$, and angles $\theta = \angle O-H\cdots O$ and $\phi = \angle H\cdots O-H$ of H-bonds obtained from the

TABLE 2: Average Parameters of Hydrogen Bonding in Liquid, Sub- and Supercritical TIP4P Water

T (K)	P (MPa)	ρ (g/cm3)	$\langle U_{HB}\rangle$ (kJ/mol)	$\langle U_{Coul}\rangle$ (kJ/mol)	$\langle U_{L-JI}\rangle$ (kJ/mol)	$\langle R_{O\cdots H}\rangle$ (Å)	$\langle\theta\rangle$ (deg)	$\langle\phi\rangle$ (deg)	$\langle n_{HBl}\rangle$	monomers (%)
298	0.1	0.99	−18.03	−24.22	6.19	1.926	160.3	99.8	3.19	0.2
573	0.95	0.06	−17.11	−21.59	4.48	2.050	151.6	96.4	0.39	63.0
573	30	0.63	−16.85	−21.63	4.78	2.027	153.6	97.7	1.61	12.2
573	50	0.67	−16.83	−21.67	4.84	2.025	153.6	97.8	1.75	10.9
573	80	0.72	−16.82	−21.70	4.88	2.023	153.6	97.7	1.77	9.5
573	100	0.75	−16.79	−21.72	4.93	2.021	153.7	97.5	1.93	8.7
673	50	0.39	−16.63	−21.17	4.54	2.049	151.8	96.8	1.05	30.8
673	80	0.54	−16.59	−21.23	4.64	2.043	152.1	96.9	1.35	21.5
673	100	0.60	−16.57	−21.25	4.68	2.041	152.2	97.0	1.36	18.5
673	130	0.66	−16.54	−21.25	4.71	2.040	152.3	97.0	1.38	16.6
673	1000	1.05	−16.34	−21.79	5.45	2.015	151.9	96.1	2.06	5.7
673	10000	1.67	−15.72	−23.79	8.07	1.956	149.2	94.5	2.82	2.35
373	100	0.98	−17.51	−23.25	5.73	1.962	157.6	98.9	2.88	0.8
473	100	0.89	−17.11	−22.36	5.25	1.996	155.4	98.2	2.23	3.3
573	100	0.75	−16.79	−21.72	4.93	2.021	153.7	97.5	1.93	8.7
673	100	0.60	−16.57	−21.25	4.68	2.041	152.2	97.0	1.36	18.5
773	100	0.44	−16.39	−20.88	4.49	2.058	150.9	96.2	0.96	34.3
1273	100	0.17	−15.79	−20.10	4.31	2.091	147.5	93.6	0.20	78.9

present MC simulations by the application of the combined distance−energy criterion are presented in Table 2, along with the resulting average number of H-bonds per water molecule and the fraction of competely nonbonded molecules (monomers) under varying thermodynamic conditions. Similar values for liquid water under ambient conditions are also given there for comparison. The energy of the H-bonding is divided into Coulomb and Lennard-Jones contributions, according to the definition of the TIP4P interaction potential. As expected, the average HB distance decreases with increasing pressure (density) along an isotherm, bringing about an increase of the repulsive LJ contribution to the pair interaction energy. At the same time however, the Coulomb contribution decreases, resulting in average total energy of H-bonding being almost density/pressure independent at a given temperature. Although some smooth variation of the average HB angles θ and ϕ is clearly observable, they too remain almost constant along an isotherm.

In general, we may conclude that the increase of temperature from ambient to supercritical affects the average energetic and spatial characteristics of H-bonding in water much more dramatically than any isothermal change in pressure or density within the range from 10 to 10 000 MPa, or from 0.03 to 1.67 g/cm^3, respectively, under supercritical conditions.

In the paper of Gorbaty and Kalinichev,[6] no definite criteria of a hydrogen bond were deliberately used for the analysis of spectroscopic and X-ray diffraction data. Instead, a quantity χ was introduced which can be considered either as the mole fraction of hydrogen bonds or as the overall degree of "hydrogen bondedness" in water under certain thermodynamic conditions. This quantity can vary from 1 to 0 for ice and very dilute vapor, respectively. In the present paper, we are using direct quantitative estimates of the average number of H-bonds per water molecule, $\langle n_{HB}\rangle$, based on our hybrid distance−energy criterion of H-bonding. Since the maximum number of ideal H-bonds per water molecule is 4 (e.g., in ice-I), these two quantities are, obviously, in a very simple relationship to each other:

$$4\chi = \langle n_{HB}\rangle \qquad (4.1)$$

Figure 10 shows the experimental estimates from the previous paper[6] (replotted in the new scale) and recent neutron diffraction data[10] along with the results of the present Monte Carlo simulations under similar thermodynamic conditions. Recent high-temperature proton NMR chemical shift measurements at pressures 10−40 MPa are also given there using the scaling factor of 3.2 for the degree of hydrogen bonding η (defined in the experimental paper[11]) and $\langle n_{HB}\rangle$. There is very good agreement between experimental data from different sources and present computer simulations. Note that above ∼700 K the NMR data correspond to densities < 0.2 g/cm^3, thus expectedly positioned below the MC results for this density, but in good agreement with low-density IR results.[29,30] Some overestimation of $\langle n_{HB}\rangle$ relative to the X-ray diffraction data[33] at lower temperatures is the direct consequence of the overestimation of the height of the $g_{OO}(r)$ first peak by the TIP4P potential data (see Figures 2 and 3). On the other hand, the value of 3.58 for $\langle n_{HB}\rangle$ derived from the neutron diffraction data[10] also seems somewhat overestimated.

From computer simulations, the general temperature dependence of $\langle n_{HB}\rangle$ is observed as a broad band between high-density (dash−dotted) and low-density (dotted) curves, asymptotically approaching zero at higher temperatures and lower densities, as previously predicted.[6] However, even at the highest temperature and the lowest density of the present simulations (Figure 10) there persists some noticeable degree of hydrogen bonding, represented, most probably, by small clusters like dimers and trimers.

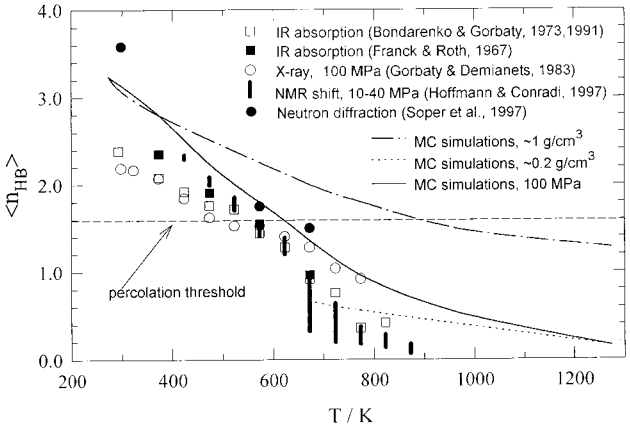

Figure 10. Temperature dependence of the average number of H-bonds per molecule, $\langle n_{HB}\rangle$ derived from the X-ray data[33] (open circles), IR absorption by ν_{OH} HDO[6,29] (open squares), IR absorption by ν_{OD} HDO[28] (filled squares), neutron diffraction[10] (filled dots), proton NMR shift[11] (vertical bars), and MC (TIP4P) simulations along the 100 MPa isobar and at two different densities.

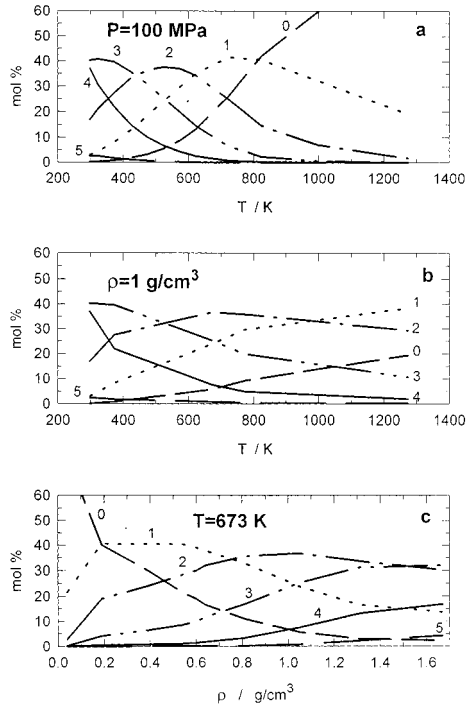

Figure 11. Distributions of molecules involved in a given number of H-bonds (numbers at the curves) in supercritical water resulting from the present MC simulations for the TIP4P intermolecular potential: (a) along an isobar of 100 MPa; (b) along an isochore of 1 g/cm^3 ; (c) along an isotherm of 673 K.

Temperature and density dependencies of fractions of water molecules having a given number of H-bonds for typical supercritical isobar, isochore, and isotherm are plotted in Figure 11 based on the present MC simulations for the TIP4P water model. For the thermodynamic conditions of neutron diffraction experiments[10] (673 K and 0.66 g/cm^3) 12% of water molecules are estimated to be involved in three H-bonds, about 70% of molecules are involved in one or two H-bonds (dimers and trimers), and only 17% represent nonbonded monomers. This picture is in good qualitative agreement with recent calculations of the water equation of state using the hydrogen-bonding lattice fluid model (LFHB)[54] and associated perturbed anisotropic chain theory (APACT).[55]

V. Conclusions

In the previous paper[6] several independent sets of experimental data were analyzed, and good consistence was demon-

strated in estimating the degree of hydrogen bonding in supercritical water. It was shown that H-bonding is still noticeable even at temperatures as high as 800 K and very low densities. In the present paper we reported the results of Monte Carlo computer simulations performed under thermodynamic conditions corresponding to the available X-ray[31−33] and neutron[10] diffraction measurements for supercritical water. We also compared these results with some other recent experimental[11] and simulated[23,34] data under simlilar thermodynamic conditions. Obviously, more experimental X-ray and neutron diffraction measurements under supercritical conditions are needed before these structural data can be used for reliable reparametrization of the available intermolecular potential functions used in computer simulations. However, even in their present form the potentials like TIP4P[36] seem to give a description of the structure and properties of supercritical water which is qualitatively, and often even quantitatively, quite consistent with available experimental data.

The detailed analysis of the picture of hydrogen bonding in supercritical water, based on the proposed intermolecular distance−energy criterion of H-bonding, demonstrated good agreement of present computer simulations with several sets of experimental data from different sources. With increasing temperature, the average number of H-bonds per water molecule decreases with the same slope for high-density (∼1 g/cm^3) as well as low-density (∼0.2 g/cm^3) supercritical water and asymptotically approaches zero at higher temperatures and lower densities, in good agreement with previous predictions.[6] Since these numbers of $\langle n_{HB} \rangle$ are well below the percolation threshold (∼1.6),[56] the continuous network of hydrogen bonds is already broken at $T = 573$ K and $\rho < 0.63$ g/cm^3 (see Figure 10 and Table 2). For temperatures above ∼873 K the continuous network is broken even for liquidlike densities above 1.0 g/cm^3. However, even at the highest temperature and the lowest density of the present simulations some degree of hydrogen bonding is still observable in the form of dimers and trimers.

For the typical supercritical conditions of $T = 673$ K and $\rho = 0.66$ g/cm^3, average hydrogen bonds are approximately 1.5 kJ/mol (or 8%) weaker, 0.1 Å (or 5%) longer, and 8° less linear, compared to those in liquid water under ambient conditions (Table 2). However, more than 40% of H-bonds are still preserved in the supercritical state according to the results of present simulations and in excellent agreement with all estimates based on experimental data from different sources.

Acknowledgment. This work would have not been possible without inspiration and continuous interest of Yu. E. Gorbaty, whose collaboration is most gratefully acknowledged. The authors are also grateful to M. A. Ricci, A. K. Soper, and M. Sprik for providing tables of their structural data, and to P. T. Cummings, G. W. Neilson, and A. K. Soper for fruitful discussions. The study was supported by the NSF (Grant EAR-9305071), Russian Basic Research Foundation (Grants 95-05-14748 and 97-03-32587), and the Civilian Research and Development Foundation (Grant RC1-170). Most calculations were performed on the IBM RS/6000 workstation granted to the authors in the framework of IBM's Shared University Research (SUR) program.

References and Notes

(1) Norton, D. L. *Annu. Rev. Earth Planet Sci*. **1984**, *12*, 155.
(2) Von Damm, K. L. *Annu. Rev. Earth Planet Sci.* **1990**, *18*, 173.
(3) Shaw, R. W.; Brill, T. B.; Clifford, A. A.; Eckert, C. A.; Franck, E. U. *Chem. Eng. News* **1990**, *69* (51), 26.
(4) Tester, J. W.; Holgate, H. R.; Armellini, F. J.; Webley, P. A.; Killiea, W. R.; Hong, G. T.; Barner, H. E. In *Emerging Technologies in Hazardous Waste Management III*; ACS Symp. Series 518, 1993; Chapter 3.
(5) Eisenberg, D.; Kautzmann, W. *The Structure and Properties of Water*; Oxford University Press: Oxford, 1969.
(6) Gorbaty, Yu. E.; Kalinichev, A. G. *J. Phys. Chem*. **1995**, *99*, 5336.
(7) Bennett, G. E.; Johnston, K. P. *J. Phys. Chem*. **1994**, *98*, 441.
(8) Soper, A. K. *J. Chem. Phys.* **1994**, *101*, 6888.
(9) Soper, A. K. *J. Phys.: Condens. Matter* **1996**, *8*, 9263.
(10) Soper, A. K.; Bruni, F.; Ricci, M. A. *J. Chem. Phys.* **1997**, *106*, 247.
(11) Hoffmann, M. M.; Conradi, M. S. *J. Am. Chem. Soc*. **1997**, *119*, 3811.
(12) Kalinichev, A. G. *Int. J. Thermophys.* **1986**, *7*, 887.
(13) Mountain, R. D. *J. Chem. Phys.* **1989**, *90*, 1866.
(14) Kalinichev, A. G. *Z. Naturforsch*. **1991**, *46a*, 433; **1992**, *47a*, 992.
(15) Cummings, P. T.; Cochran, H. D.; Simonson, J. M.; R.E.Mesmer, R. E.; Karaborni, S. *J. Chem. Phys.* **1991**, *94*, 5606.
(16) Kalinichev, A. G.; Heinzinger, K. In Thermodynamic Data: Systematics and Estimation, Saxena, S. K., Ed.; Advances in Physical Geochemistry, Vol. 10; Springer: New York, 1992, Chapter 1.
(17) Brodholt, J.; Wood, B. *J. Geophys. Res.* **1993**, *98B*, 519.
(18) Kalinichev, A. G. *Ber. Bunsen-Ges. Phys. Chem.* **1993**, *97*, 872.
(19) Kalinichev, A. G.; Bass, J. D. *Chem. Phys. Lett.* **1994**, *231*, 301.
(20) Chialvo, A.; Cummings, P. T. *J. Chem. Phys.* **1994**, *101*, 4466.
(21) Mizan, T. I.; Savage, P. E.; Ziff, R. M. *J. Phys. Chem*. **1994**, 98, 13067.
(22) Löffler, G.; Schreiber, H.; Steinhauser, O. *Ber. Bunsen-Ges. Phys. Chem*. **1994**, *98*, 1575.
(23) Kalinichev, A. G.; Heinzinger, K. *Geochim. Cosmochim. Acta* **1995**, *59*, 641.
(24) Mountain, R. D. *J. Chem. Phys.* **1995**, *103*, 3084.
(25) Kalinichev, A. G.; Bass, J. In *Proceedings of the 12th International Conference on the Properties of Water and Steam;* White, H. J., Jr., Sengers, J. V., Neumann, D. B., Bellows, J. C., Eds.; Begell House: New York, 1995; p 245.
(26) Mizan, T. I.; Savage, P. E.; Ziff, R. M. *J. Phys. Chem*. **1996**, *100*, 403.
(27) Chialvo, A.; Cummings, P. T. *J. Phys. Chem*. **1996**, *100*, 1309.
(28) Franck, E. U.; Roth, K. *Discuss Faraday Soc*. **1967**, *42*, 108.
(29) Bondarenko, G. V.; Gorbaty, Yu. E. *Dokl. Phys. Chem.* **1973**, *210*, 369.
(30) Bondarenko, G. V.; Gorbaty, Yu. E. *Mol. Phys.* **1991**, *74*, 639.
(31) Gorbaty, Yu. E.; Demianets, Yu. N. *J. Struct. Chem.* **1983**, *24*, 365.
(32) Gorbaty, Yu. E.; Demianets, Yu. N. *J. Struct. Chem.* **1983**, *24*, 716.
(33) Gorbaty, Yu. E.; Demianets, Yu. N. *Chem. Phys. Lett.* **1983**, *100*, 450.
(34) Fois, E. S.; Sprik, M.; Parrinello, M. *Chem. Phys. Lett.* **1994**, *223*, 411.
(35) Allen, M. P.; Tildesley, D. J. *Computer Simulation of Liquids*; Oxford University Press: New York, 1987.
(36) Jorgensen, W. L.; Chandrasekhar, J.; Madura, J. D.; Impey, R. W.; Klein, M. L. *J. Chem. Phys.* **1983**, *79*, 926.
(37) Kalinichev, A. G.; Bass, J. D. In preparation, 1997.
(38) Saul, A.; Wagner, W. *J. Phys. Chem. Ref. Data* **1989**, *18*, 1537.
(39) De Pablo, J. J.; Prausnitz, J. M. *Fluid Phase Equilib.* **1989**, *53*, 177.
(40) Reimers, J. r.; Watts, R. O.; Klein, M. L. *Chem. Phys.* **1982**, *64*, 95
(41) Ruff, I.; Diestler, D. J. *J. Chem. Phys.* **1990**, *93*, 2032.
(42) Guissani, Y.; Guillot, B. *J. Chem. Phys.* **1993**, *98*, 8221.
(43) Berendsen, H. J. C.; Grigera, J. R.; Straatsma, T. P. *J. Phys. Chem*. **1987**, *91*, 6269.
(44) Bopp, P.; Jancsó, G.; Heinzinger, K. *Chem. Phys. Lett.* **1983**, *98*, 129.
(45) Bruni, F.; Ricci, M. A.; Soper, A. K. *Phys. Rev. B* **1996**, *54*, 11876.
(46) Mezei, M.; Beveridge, D. L. *J. Chem. Phys.* **1981**, *74*, 622.
(47) Belch, A. C.; Rice, S. A.; Sceats, M. G. *Chem. Phys. Lett.* **1981**, *77*, 455.
(48) Pálinkás, G.; Bopp, P.; Jancsó, G.; Heinzinger, K. *Z. Naturforsch*. **1984**, *39a*, 179.
(49) Stillinger, F. H.; Rahman, A. *J. Chem. Phys.* **1972**, *57*, 1281.
(50) Rapaport, D. C. Mol. Phys. **1983**, *50*, 1151.
(51) Walrafen, G. E.; Chu, Y. C. *J. Phys. Chem*. **1995**, *99*, 11225.
(52) Kalinichev, A. G.; Heinzinger, K. In preparation.
(53) Svishchev, I. M.; Kusalik, P. G. *J. Chem. Phys.* **1993**, *99*, 3049.
(54) Gupta, R. B.; Panayiotou, C. G.; Sanches, I. C.; Johnston, K. P. *AIChE J.* **1992**, *38*, 1243.
(55) Smits, P. J.; Economou, I. G.; Peters, C. J.; de Swaan Arons, J. *J. Phys. Chem.* **1994**, *98*, 12080.
(56) Blumberg, R. L.; Stanley, H. E.; Geiger, A.; Mousbach, P. *J. Chem. Phys.* **1984**, *80*, 5230